

# A Dual-Wideband Crossed Elliptical Disc Antenna with Reconfigurable Radiation Patterns for Multiband Applications

**Abstract.** This paper presents the design of a crossed elliptical disc antenna with two broad operating bandwidths, which covers several widely-employed frequency standards: IEEE 802.11b/g/n (WLAN), IEEE 802.16 (WiMAX), GSM/UMTS and LTE. The antenna comprises a crossed elliptical radiator, step-fed transitions, L-shaped slits and split (defected) circular ground-planes. Moreover, the antenna is equipped with four switches to have reconfigurable options for the conical-beam radiation patterns. The fabricated antenna prototype offers the dual broad-bandwidths of 1.17 GHz (1.88-3.05 GHz) and 2.05 GHz (4.67-6.72 GHz), which cover the required frequency bands. The peak gains of the normal-mode conical beams are 3.05 and 5.91 dBi at 2.45 GHz and 5.5 GHz, respectively. It has the advantage of having main-beam directions pointing to nearly the same tilted angle for both operating frequencies, which is very useful for most simultaneous dual-band operations and ceiling-mounted installations.

**Streszczenie.** W artykule zaprezentowano projekt eliptycznej anteny o dwóch pasmach częstotliwości obsługującej zakresy zgodnie ze standardem IEEE 802.11b/g/n. Wykonany model anteny obsługuje pasma 1.88 – 3.05 GHz oraz 4.67 – 6.72 GHz. Wzmocnienie wynosiło 3.05 i 5.91 dBi. Dwupasmowa antena szerokopasmowa z eliptycznym dyskiem z możliwością konfiguracji so wielopasmowych zastosowań.

**Keywords:** dual-wideband antenna, elliptical disc, reconfigurable radiation pattern, conical beam

**Słowa kluczowe:** antena szerokopasmowa, antena dwuzakresowa, antena eliptyczna.

## Introduction

Contrary to the main conventional wired networks, the wireless local area networks (WLAN) and other wireless technologies provide the convenience of user's mobility, accessibility ease and cost-effectiveness, contributing to the ever-increasing adoption of the wireless communication in innumerable applications. Some wireless networks demand multiple frequency standards, thereby rendering the multi-band technology highly desirable. Modern antennas for wireless systems should thus incorporate the multi-band features. At present, there are two WLAN standards commonly adopted worldwide i.e. IEEE 802.11b/g/n and IEEE 802.11a; as well as some other modern technologies, e.g., IEEE 802.16 (WiMAX), GSM/UMTS and LTE.

A wide variety of techniques and elements have been implemented on the antenna body to achieve the multi-band characteristics. For instant, many multi-radiator elements proposed in [1] using three sets of radiating elements to cover three operating bands: 900 MHz, 2 GHz, and 3.5/5 GHz; in [2] with three sets of printed monopole structures to cover the 2.4 GHz, 3.5 GHz and 5 GHz bands for WLAN/WiMAX applications; and the dual-band patch antenna designed for the GPS (1575 MHz) and WLAN (2.4 GHz) applications by stacking a square patch with a corner-truncated square-ring patch [3]. Some other recent approaches were also reported, using metamaterial/EBG, defected ground and/or multi-branch monopole structures, to obtain antennas with multi-band characteristics for applications in many widely-used standards, e.g. for WLAN/WiMAX bands [4-6, 8]; C/X bands [5]; LTE/WWAN [7-8]; and 5G mobile technology [9].

Furthermore, several attempts have been made upon reconfigurable antennas. Some were for reconfiguring the radiation patterns, beam-width and main beam directions, such as use of mechanically moving reflectors and tuning material properties [10-11], electrically and optically controls [12-13]. There were also topics regarding frequency and bandwidth reconfiguration using fluid switches [14], and electrically controllable switches [15-16], which supported a wide variety of applications. Additionally, the polarization of antennas is also the trend of reconfiguration, such as for obtaining: the antenna with multi-polarization by switching difference phases of the feeding arms [17], selectable circularly-polarized antennas [18-19], and reconfigurable polarization of the broadband antenna [20].

In this current research, we propose an antenna with two broad bandwidths for mainly supporting IEEE 802.11b/g/n (WLAN 2.4/5 GHz) and IEEE 802.16 (WiMAX 2.3/2.5/5.8 GHz) frequency standards, as well as other bands: GSM/UMTS (1.9/2.1 GHz) and LTE (2.3/2.5 GHz). The dual-wideband property is realized by incorporating a crossed elliptical radiator, a step-fed transition and L-shaped slits. The ground-plane structures with gaps (splits) are utilized for impedance matching and balancing, and also for reconfiguring the conical-beam peaks by using switches. The proposed antenna is realizable for large-area indoor signal distributions with ceiling-mounted installation, where the azimuthally symmetric or asymmetric (adjustable) around a center point are required for both wide operating bandwidths. In the study and design, the simulations are performed by using the CST Microwave Studio software.

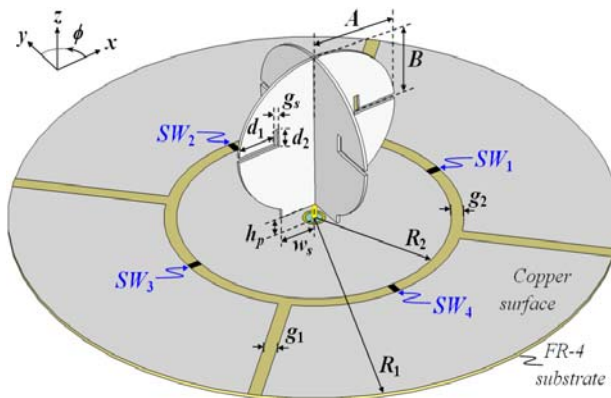


Fig.1. Antenna structure

## Antenna Geometry

In Fig. 1, a general antenna structure is illustrated where  $A$  and  $B$  are the major and minor axes of the copper elliptical disc with the thickness of 1 mm joining to the tip of the feeding probe of height,  $h_p$ . At the bottom of the ellipse, there is the one-step feeding transition with the step width of  $w_s$ . On the elliptical disc, four L-shaped slits are cut with two orthogonal slits of lengths  $d_1$  and  $d_2$ , and the slit gap of  $g_s$ . The circular ground plane, made of a single-sided FR-4 PCB with the thickness of 1.6 mm, dielectric constant of 4.3,

consists of a conventional ground plane and four circular-sector parasitic grounds; all are defined by the radii of  $R_1$  and  $R_2$ , and separated by the gaps of  $g_1$  and  $g_2$ . Finally, a simple model of 3.5-mm SMA connector is also included in the ground plane, and being fed by an excitation source.

## Antenna Design and Parametric Study

### A) Design of Initial Parameters

Prior to proceeding in the numerical simulation, good initializing parameters of the antenna are essential to diminish the computation and optimization time. The first set of parameters to be determined is relating to the ground plane. The suitable outer ( $R_1$ ) and inner ( $R_2$ ) radii are initially predicted based on their respective diameters of one wavelength ( $\lambda_1 \cong 122.44$  mm and  $\lambda_2 \cong 54.55$  mm) of the expected first and second resonant frequency ( $f_1 = 2.45$  GHz and  $f_2 = 5.5$  GHz) respectively, as shown below:

$$(1) \quad R_1 = \lambda_1/2, \quad R_2 = \lambda_2/2$$

Thus, the first estimation of both ground-planes' radii can be obtained around  $R_1 \cong 61.22$  mm and  $R_2 \cong 27.27$  mm, while all gaps ( $g_1$  and  $g_2$ ) are firstly assumed 1 mm. The feeding-probe height ( $h_p$ ) is initially set to 3 mm because the constraint of the practical value is between 2 and 4 mm.

The parameters of the crossed elliptical radiator may be initially estimated based on the resonant frequency by equating the approximate circumference of the elliptical disc to one wavelength ( $\lambda_1$ ) of the first resonant frequency as:

$$(2) \quad k_d \cdot 2\pi \sqrt{\frac{A^2 + B^2}{2}} = \lambda_1$$

where  $k_d$  is the compensation factor for the approximate circumference of the ellipse, including effects of the added step feeding and coupling of the crossed disc. Next, by introducing the axial ratio,  $AR = A/B$  (for  $A > B$ ), equation (2) can be solved for the minor axis ( $B$ ) as follows:

$$(3) \quad B = \frac{\lambda_1}{k_d \cdot \pi \sqrt{2(AR^2 + 1)}}$$

Then the major axis ( $A$ ) can be determined by  $A = AR \times B$ . As of the initialization, the selected values of  $AR = 4/3$  and  $k_d = 1$ , along with the calculated  $\lambda_1$ , result in  $B \cong 16.54$  mm and  $A \cong 22.05$  mm. Also,  $w_s$  is firstly assumed 10 mm.

Finally, the L-shaped slits (see Fig. 1) are employed to control the center of the notch frequency in the middle band. For the selected notch frequency of  $f_n = (f_1 + f_2)/2 = 3.975$  GHz, segment lengths of the L-shaped slits ( $d_1$  and  $d_2$ ) may be evaluated by using the relation between the electrical length along the open-ended L-shaped path and the half-wavelength ( $\lambda_n/2$ ) of the notch frequency ( $f_n$ ) as:

$$(4) \quad k_s \cdot 2(d_1 + d_2) + g_s = \lambda_n/2 \rightarrow d_2 = \frac{\lambda_n/2 - g_s}{2k_s(LR + 1)}$$

where  $k_s$  is the correction factor for the approximate notch frequency of the slits.  $LR$  is the length ratio of the L-shaped slit (i.e.  $d_1/d_2$ , for  $d_1 > d_2$ ). Then the longer segment ( $d_1$ ) can be determined from  $d_1 = LR \times d_2$ . By specifying the initial value of  $LR = 3/1$  and  $k_s = 1$ , with the calculated  $\lambda_n \cong 75.47$  mm, equation (3) and the definition of  $LR$  yield  $d_2 \cong 4.59$  mm and  $d_1 \cong 13.78$  mm. The gap ( $g_s$ ) of the slits is initially

assumed 1 mm. The predicted parameters above are being used to initiate the first round of simulation, then they are to be fine-tuned later in the following parametric optimization.

### B) Parametric Study

The first set of parameters to be study is relating to the feeding of the antenna, i.e.  $h_p$  and  $w_s$ , since it significantly affects the impedance matching of the antenna to the 50- $\Omega$  characteristic impedance. The impedance matching is considered and visualized, here, as  $|S_{11}|$  (magnitude) in dB.

In Fig. 2, the feeding-probe height ( $h_p$ ) is varied in its practical range from 2 to 4 mm. It is obvious that the feeding height has a strong effect on the impedance matching. Good impedance characteristics, i.e. the best matching points (minima of  $|S_{11}|$ ) and bandwidths, is observed between 3.0 and 3.5 mm. So the new value of  $h_p$  of 3.25 mm is taken and being used in the next parametric study.

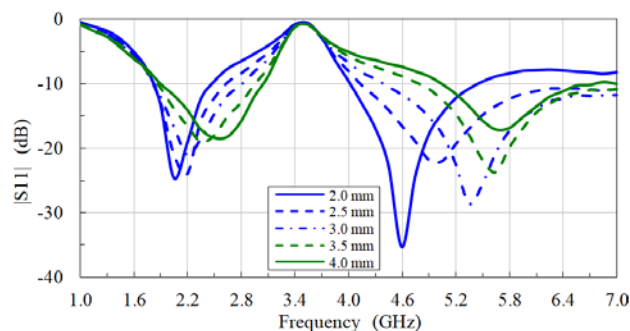


Fig.2.  $|S_{11}|$  for different values of  $h_p$

Next, the width ( $w_s$ ) of the one-step feeding transition is investigated as shown in Fig. 3. It is a conclusive proof that the step feeding can be effectively employed to limit the ultra-wideband characteristic of the elliptical disc, in the higher operating band (5.5-GHz band). As the second stage of prediction, the best impedance characteristic is expected where  $w_s$  is in the range from 10 to 11 mm. Thus, the new value of  $w_s = 10.5$  mm is selected for the next simulation.

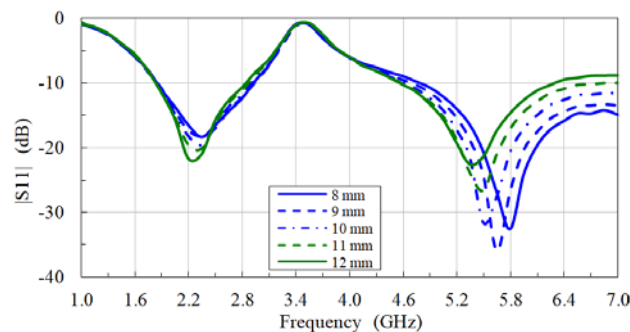


Fig.3.  $|S_{11}|$  for different values of  $w_s$

The second set of parameters to be study involves the crossed elliptical disc, i.e.  $k_d$  and  $AR$ . These key parameters are the main contribution towards achieving the broad-bandwidth characteristic.

Fig. 4 illustrates the impedance matching as a function of the compensation factor for the crossed elliptical disc ( $k_d$ ). It can be observed that the initial value of  $k_d = 1$  did not exactly result in the resonant frequency (dip of  $|S_{11}|$  curve) at 2.45 GHz due to the approximation of the elliptical perimeter, the step feeding and coupling of the crossed disc, as mentioned earlier in the previous sub-section. By examining the results, the appropriate value of  $k_d$  should be around 1.0, to maintain the best  $|S_{11}|$  dips at both 2.45 and 5.5 GHz, and to be fine-tuned in the optimization procedure.

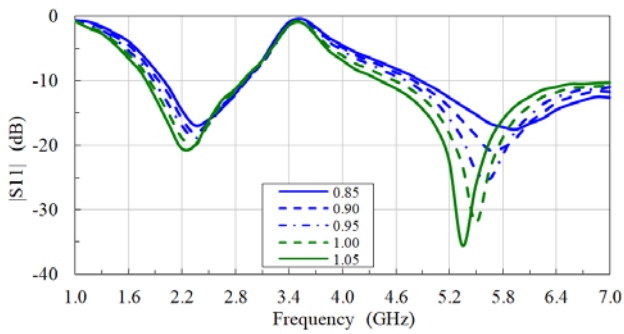


Fig.4.  $|S_{11}|$  for different values of  $k_d$

Next, the axial ratio ( $AR$ ) of the elliptical disc is studied as shown in Fig. 5. From the  $|S_{11}|$  curves, it can be clearly seen that  $AR$  contributes to the remarkable impedance matching of both operating bands, and can be utilized to compromise and balance the best-matched points at 2.45 and 5.5 GHz. The best impedance matching characteristic is forecasted for  $AR$  between 1.33 and 1.43. Then the average value of  $AR = 1.38$  is estimated at this stage.

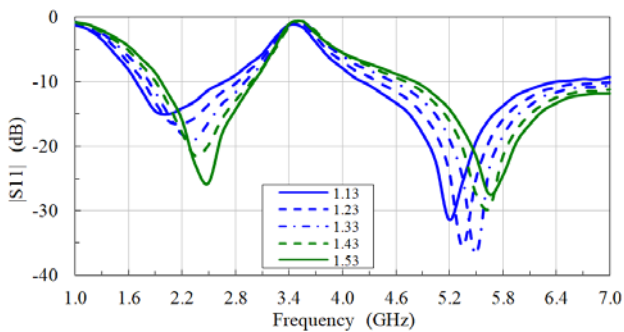


Fig.5.  $|S_{11}|$  for different values of  $AR$

The effects of the third set of parameters to be enquired into concerns the L-shaped slit, i.e.  $k_s$  and  $LR$ . Generally, a slit generates a notch frequency that may be applied to control the rejection of certain bandwidth, resulting in multiband applications.

Fig. 6 presents the impedance matching by varying the correction factor of the L-shaped slit ( $k_s$ ). It reveals that the initial value of  $k_s = 1$  did not yield the notch frequency at 3.975 GHz as predicted because of the coupling effects of the crossed disc and nearby slits. The reasonable value of  $k_s$  should be nearly 0.95 to obtain the best  $|S_{11}|$  condition at both 2.45 and 5.5 GHz.

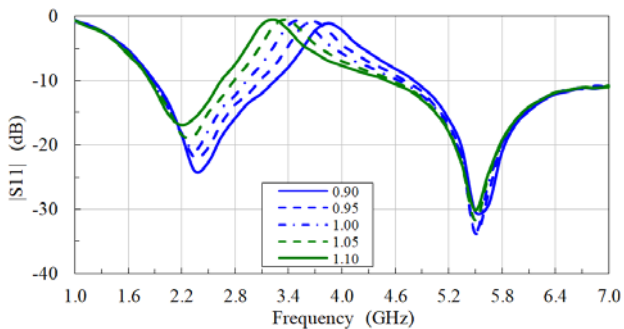


Fig.6.  $|S_{11}|$  for different values of  $k_s$

Next, the length ratio ( $LR$ ) of the L-shaped slit is examined as shown in Fig. 7. From the  $|S_{11}|$  curves, it can be observed that  $LR$  offers a slight impedance balancing effect. Although the satisfactory balance of the impedance

is displayed at  $LR = 1$ , the value of  $LR$  greater than 2 should be maintained due to the practical structure of the slit being cut on the thin elliptical surface.

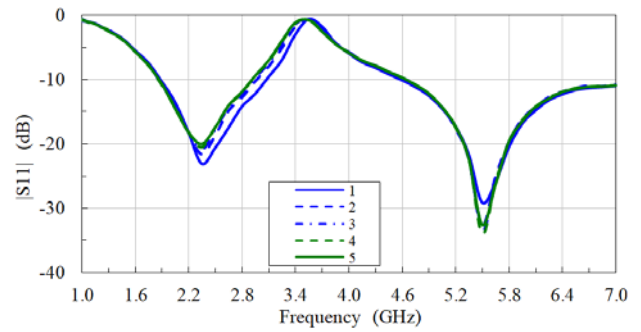


Fig.7.  $|S_{11}|$  for different values of  $LR$

The last set of parameters of the ground planes, i.e.  $R_1$ ,  $R_2$  and  $g_2$ , are altered to inspect the impedance matching characteristic, using the new current values of  $AR$  and  $k_d$ .

Fig. 8 displays the impedance matching as a function of  $R_1$ . It is discovered that  $R_1$  may be useful when the resonant frequencies (dip of  $|S_{11}|$ ) of both bands are required to be equally shifted. It should be noted that large expansion of  $R_1$  is undesirable, governed by the overall size of the antenna. The reasonable value of  $R_1$  should lie somewhere in the range from 58.2 to 61.3 mm, and be optimized later.

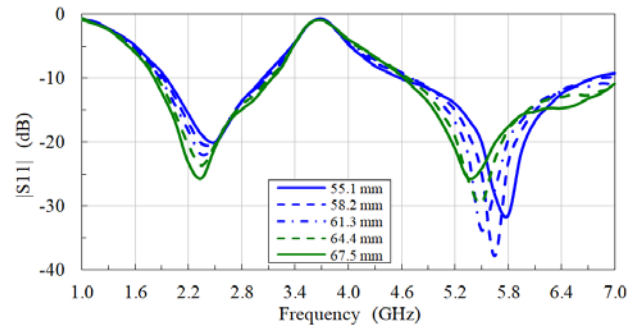


Fig.8.  $|S_{11}|$  for different values of  $R_1$

Fig. 9 illustrates the  $|S_{11}|$  curves as the radius ( $R_2$ ) of the conventional inner ground-plane is varied. It can be seen that this parameter significantly affects the higher band (5.5 GHz), thus it may be considered as another degree of freedom to tune the best matching point of the higher band. The best impedance matching characteristic is observed for  $R_2$  between 27.1 and 28.0 mm.

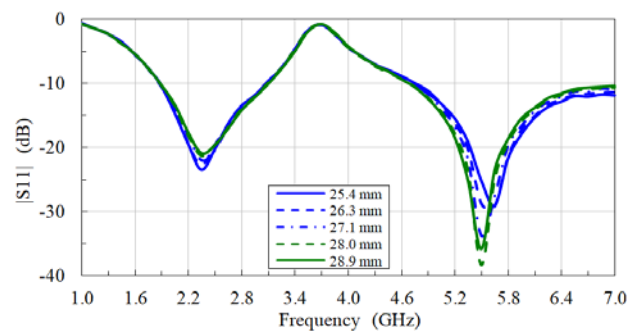


Fig.9.  $|S_{11}|$  for different values of  $R_2$

Various values of the annular gap ( $g_2$ ) separating the conventional inner and parasitic outer ground-planes result in the  $|S_{11}|$  curves as in Fig. 10. It is noticeable that the gap helps to improve the impedance balancing effectively. Even

though the results of antenna gain affected by  $g_2$  are not shown here, the analysis was performed and concluded that increasing the gap led to the reduction of antenna gain. The suitable value of  $g_2$  should be between 1 and 2 mm to preserve the best match points for both 2.45 and 5.5 GHz.

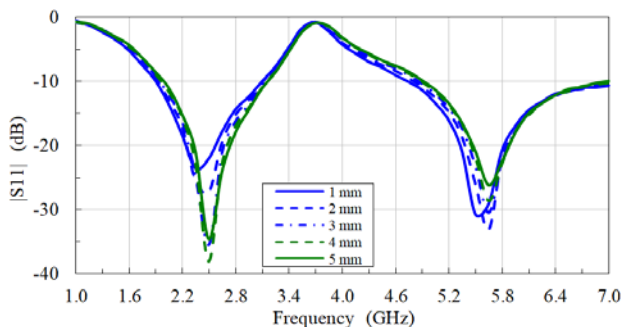


Fig.10.  $|S_{11}|$  for different values of  $g_2$

Other small-value parameters, i.e.  $g_s$  and  $g_1$ , have been investigated and found that they have slight effects on antenna's main characteristics, so they are being used later as fine-tuning parameters for the optimization procedure.

Finally, in order to automate the simulation process and consideration of the main parameters simultaneously, the built-in Genetic Algorithm optimizer is utilized to obtain the optimized values of the proposed antenna based on the bandwidth and impedance matching criteria constrained by the coverage of the two aforementioned broad bandwidths. After the fine-tuning optimization procedure, the optimized values of physical parameters are tabulated in Table 1 and computed for the best matching ( $|S_{11}|$ ) condition in Fig. 11.

Table 1. Optimized physical parameters

Parameter	Measure (mm)	Parameter	Measure (mm)
$A$	23.71	$g_s$	1.20
$B$	17.18	$R_1$	60.95
$h_p$	3.44	$R_2$	27.37
$w_s$	10.52	$g_1$	1.10
$d_1$	11.86	$g_2$	1.45
$d_2$	5.22		

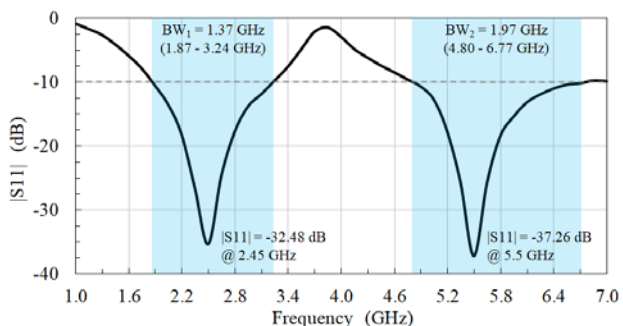


Fig.11.  $|S_{11}|$  characteristic for the optimized physical parameters

### C) Pattern Reconfiguration

Reconfigurable radiation patterns of the antenna are accomplished by alternating the closed and open states of the four switches (see Fig. 1). There are five sets of the switch states that generate distinct styles of radiation patterns shown in Table 2. Although there are many other possible combining sets of closed/open states, some sets have similar pattern styles. For example, any case with a single closed switch will result in similar pattern-style to that

of Case A except that the main beam is rotated. In addition, when all switches are in closed states, the impedance matching of the first band is deteriorated rapidly due to the resistance and reactance overloading from the four parasitic ground planes. Thus, the case of four closed switches is not applicable for the purpose of pattern reconfiguration.

Table 2. States of the switches that generate distinct pattern styles

Case	SW <sub>1</sub>	SW <sub>2</sub>	SW <sub>3</sub>	SW <sub>4</sub>
A (Normal mode)	Open	Open	Open	Open
B	Closed	Open	Open	Open
C	Closed	Closed	Open	Open
D	Closed	Closed	Closed	Open
E	Closed	Open	Closed	Open

In Fig. 12 (a) through (e), five distinct pattern styles are presented for all cases from Table 2 along with their respective  $|S_{11}|$  curves. Each polar plot is displayed in the range from 0 to -3 dB to enhance the visibility of the peak distribution at the main conical beam. The pattern at each frequency is normalized by its own maximum gain ( $G_{max}$ ) at the fixed main-beam direction ( $\theta_{max}$ ) and varied in the  $\phi$ -direction, i.e. the plots of both frequencies are not relative.

The characteristics of the conical-beam patterns at  $\theta_{max}$  are observed and summarized below:

Case A: For 2.45-GHz,  $G_{max} = 2.93$  dBi, the main conical beam is tilted to  $\theta_{max} = 47^\circ$  degrees and omnidirectional, while for 5.5-GHz,  $G_{max} = 5.82$  dBi, the main beam direction is  $\theta_{max} = 45^\circ$  degrees and nearly omnidirectional with slight effects from the four parasitic ground-planes.

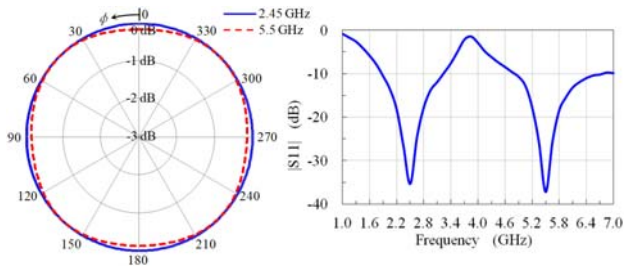
Case B: For 2.45-GHz,  $G_{max} = 3.33$  dBi, the main conical beam is tilted to  $\theta_{max} = 46^\circ$  degrees and pointing in the direction opposite to the closed switch (SW<sub>1</sub>), while for 5.5-GHz,  $G_{max} = 6.02$  dBi, the main beam direction is  $\theta_{max} = 46^\circ$  degrees and the pointing direction is similar to that of 2.45-GHz case with three split main beams.

Case C: For 2.45-GHz,  $G_{max} = 3.35$  dBi, the main conical beam is tilted to  $\theta_{max} = 42^\circ$  and pointing in the direction of the two closed switches (SW<sub>1</sub> to SW<sub>2</sub>). For 5.5-GHz,  $G_{max} = 6.29$  dBi, the direction of main beam is  $\theta_{max} = 44^\circ$  degrees and the pointing direction is similar to that of 2.45-GHz case with split two main beams and three minor beams.

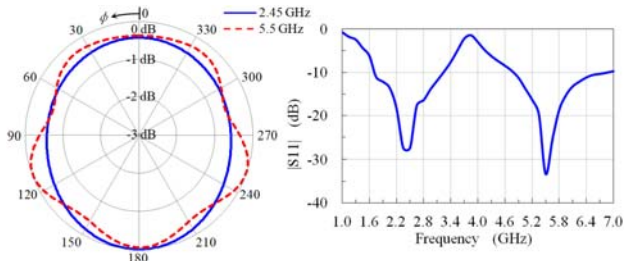
Case D: For 2.45-GHz,  $G_{max} = 3.23$  dBi, the main conical beam is tilted to  $\theta_{max} = 46^\circ$  degrees and pointing in the direction of the three closed switches (SW<sub>1</sub> to SW<sub>3</sub>), while for 5.5-GHz,  $G_{max} = 6.17$  dBi, the main beam direction is  $\theta_{max} = 46^\circ$  degrees and the pointing direction is similar to that of 2.45-GHz case with four split main beams.

Case E: For 2.45-GHz,  $G_{max} = 3.19$  dBi, the main conical beam is tilted to  $\theta_{max} = 47^\circ$  degrees and nearly bidirectional pointed in the direction of the two closed switches (SW<sub>1</sub> and SW<sub>3</sub>), while for 5.5-GHz,  $G_{max} = 6.79$  dBi, the main beam direction is  $\theta_{max} = 47^\circ$  degrees and the pointing direction is similar to that of 2.45-GHz case with remarkable bidirectional pattern.

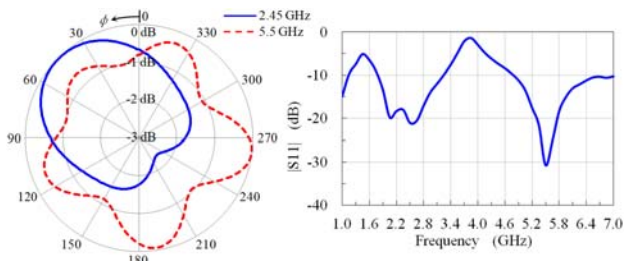
It is noticeable, for each case and each pair of both frequencies (2.45 and 5.5 GHz), that the difference of  $\theta_{max}$  is within 2 degrees. Also, from Fig. 12 (a) through (e), it is obvious that all cases are applicable because all  $|S_{11}|$  curves still provide the bandwidth coverage as required.



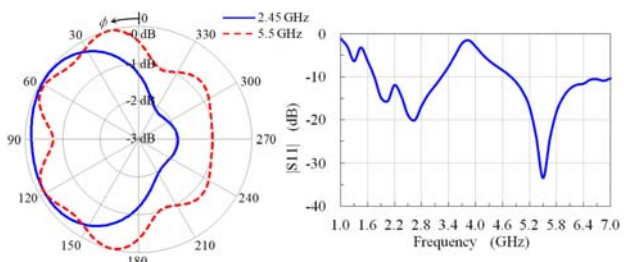
(a) Case A



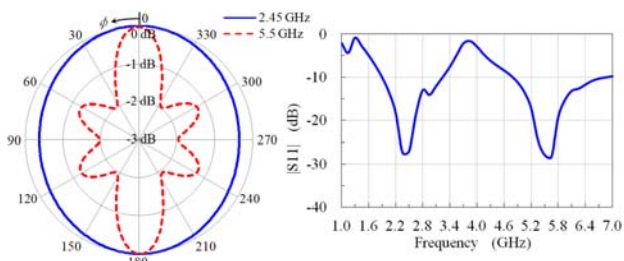
(b) Case B



(c) Case C



(d) Case D



(e) Case E

Fig.12. Reconfigurable pattern styles and their respective  $|S_{11}|$

### Experimental Results and Discussion

In order to verify the feasibility of the proposed antenna optimized by the simulation, the antenna prototype has been fabricated as shown in Fig. 13. The switch elements are of low-profile plastic-pakaged type to minimize the effects of reflection and diffraction of the radiated waves. Alternatively, some electrically controlled switches may also be utilized for this antenna structure, at the expense of

increase in the insertion loss and complexity, e.g., using RF switches and/or PIN-diode circuits with DC voltage sources, capacitors (for DC blocking) and inductors (for RF blocking).



Fig.13. Photograph of the fabricated antenna prototype

The measured results of  $|S_{11}|$  curves are illustrated in Fig. 14, for all cases from Table 2, along with the minimum bandwidths (Min. BW) noted for both operating bands. When compared with the  $|S_{11}|$  from Fig.12, it is observed that trends of the results are in good agreement with some degree of discrepancy due to the fabrication tolerance.

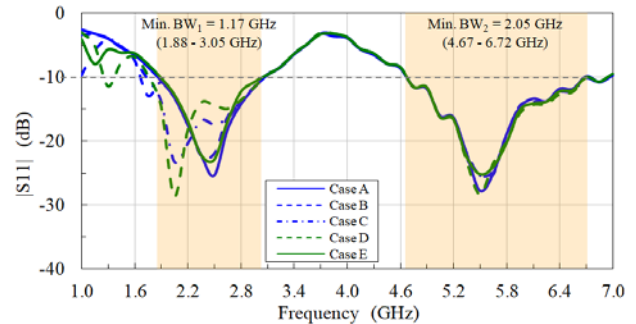
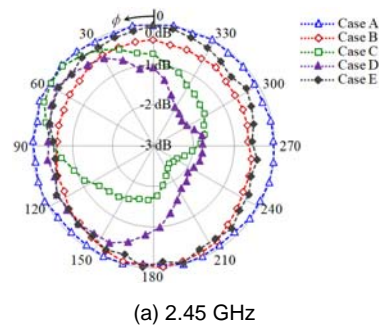
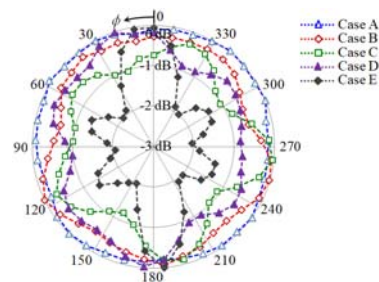


Fig.14. Measured  $|S_{11}|$  characteristics for all cases from Table 2

For the radiation patterns, the measurement of the main conical beams, fixed at the main-beam direction ( $\theta_{max}$ ) and varying  $\phi$ , has been carried out and depicted in Fig. 15. The pattern forms (styles) in Fig. 15 and Fig. 12 are agreed well.



(a) 2.45 GHz



(b) 5.5 GHz

Fig.15. Measured patterns at the main conical-beam directions

The radiation patterns in the  $x$ - $z$  (E) and  $x$ - $y$  (H) planes have also been simulated and measured as shown in Fig. 16, for the normal-mode case. They are in good agreement, with some slight effects of the diffractions at the four switches.

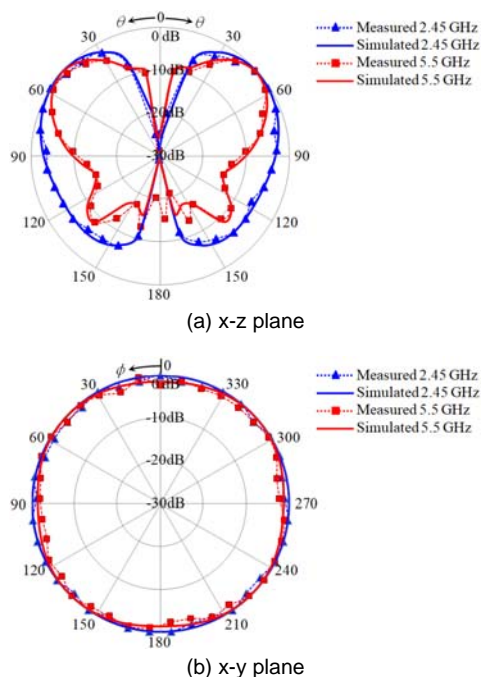


Fig.16. Measured and simulated patterns in the  $x$ - $z$  and  $x$ - $y$  planes

Finally, the peak (maximum) gains of the antenna from the measurement and simulation at some selected frequencies, for the normal-mode case, are tabulated in Table 3. The results show good agreement because loss factors in the copper and FR-4 materials were also considered in the simulation, reflecting the realized gains.

Table 3. Measured and simulated maximum gains

Frequency (GHz)	Measured (dBi)	Simulated (dBi)
2.1	2.08	2.19
2.3	2.65	2.77
2.45	3.05	3.18
5.2	5.31	5.45
5.5	5.91	6.07
5.8	6.01	6.19

## Conclusions

The crossed elliptical disc antenna was proposed for applications in two broad operating bandwidths, covering a variety of frequency standards such as WLAN, WiMAX, GSM/UMTS and LTE. The step feeding transitions and the L-shaped slits were utilized to control the dual-broadband characteristic. Additionally, on the split circular ground-planes, four mechanical switches were employed to have the reconfigurable conical-beam patterns. The fabricated antenna provides two broad bandwidths of 1.17 GHz and 2.05 GHz. The normal-mode peak gains are 3.05 and 5.91 dBi at 2.45 GHz and 5.5 GHz, respectively. The proposed reconfigurable antenna has the advantage of having main-beam directions pointing to nearly the same tilted angle for both main operating frequencies, which is a feasible candidate for most dual-broadband operations.

**Authors:** Ekajit Khoomwong, Department of Telecommunications Engineering, Faculty of Engineering, King Mongkut's Institute of Technology Ladkrabang, Bangkok, 10250, Thailand. E-mail:

[ekajitkh@gmail.com](mailto:ekajitkh@gmail.com); Chuwong Phongcharoenpanich, Department of Telecommunications Engineering, Faculty of Engineering, King Mongkut's Institute of Technology Ladkrabang, Bangkok, 10250, Thailand. E-mail: [chuwong.ph@kmitl.ac.th](mailto:chuwong.ph@kmitl.ac.th).

## REFERENCES

- [1] LIU H., LI R., PAN Y., et al, A multi-broadband planar antenna for GSM/UMTS/LTE and WLAN/WiMAX handsets, *IEEE Trans. Antenn. Propag.*, 62(2014), No. 5, 2856-2860.
- [2] LI R. L., QUAN X. L., CUI Y. H., et al, Directional triple-band planar antenna for WLAN/WiMAX access points, *IET Electron. Lett.*, 48(2012), No. 6, 305-306.
- [3] MA S.-L., ROW J.-S., Design of single-feed dual-frequency patch antenna for GPS and WLAN applications, *IEEE Trans. Antenn. Propag.*, 59(2011), No. 9, 3433-3436.
- [4] Smyth B. P., Barth S., Lyer A. K., Dual-band microstrip patch antenna using integrated uniplanar metamaterial-based EBGs, *IEEE Trans. on Antenn. and Propag.*, 64(2016), No. 12, 5046-5053.
- [5] Khanna P., Shinghal K., Kumar A., Multi-band annular ring microstrip antenna with defected ground structure for wireless communication, *Inter. Jour. of Compu. Applica.*, 135(2016), No.2, 19-25.
- [6] Lamultree S., Jansri C., Phongcharoenpanich C., Gain improvement of dual-band circular monopole antenna for 2.45/5.5 GHz WLAN applications, *Przegląd Elektrotechniczny*, 95(2019), nr 5, 157-160.
- [7] Cheng T. H., Tsai J. K., Hung W. T., Chen S. Y., Dual-band handset antenna based on multi-branch monopole for LTE/WWAN applications, *Proceedings of the International Symposium on Antennas and Propagation (ISAP 2016)*, Okinawa, Japan, 24-28 October 2016.
- [8] Guo D., He K., Zhang Y., Song M., A multiband dual-polarized omnidirectional antenna for indoor wireless communication systems, *IEEE Antenn. and Wireless Propag. Lett.*, 16(2017), 290-293.
- [9] Araujo H. X., Freitas A. E., Prata D. N., et al, A multiband antenna design comprising the future 5G mobile technology, *Przegląd Elektrotechniczny*, 95(2019), nr 2, 108-111.
- [10] Ma C., Li H., Zhang B., et al, Reconfigurable diffractive antenna with three degrees of freedom the main beam, *Electronics Lett.*, 53(2017), 1452-1454.
- [11] Basbug S., Design and synthesis of antenna array with movable elements along semicircular paths, *IEEE Antenn. and Wireless Propag. Lett.*, 16(2017), 3059-3062.
- [12] Zhang Y., Lin S., Yu S., et al, Design and analysis of optically controlled pattern reconfigurable planar Yagi-Uda antenna, *IET Microw., Antenn. & Propag.*, 12(2018), 2053-2059.
- [13] Pant A., Kumar L., Gupta R. D., et al, Investigation on non-linear aspects of pattern reconfigurable hexagon shaped planar loop antenna, *IET Microw., Antenn. & Propag.*, 13(2019), 1158-1165.
- [14] Borda-Fortuny C., Tong K.-F., et al, Al-Armaghany A., A low-cost fluid switch for frequency-reconfigurable vivaldi antenna, *IEEE Antenn. and Wireless Propag. Lett.*, 16(2017), 3151-3154.
- [15] Feng B., Luo T., Zeng Q., et al, Frequency reconfigurable antenna with triple linear polarisation and wide H-plane characteristic for future smart communications, *IET Microw., Antenn. & Propag.*, 12(2018), 2276-2284.
- [16] Wen Z., Tang M.-C., Ziolkowski R. W., Band- and frequency-reconfigurable circularly polarised filtenna for cognitive radio applications, *IET Microw., Antenn. & Propag.*, 13(2019), 2276-2284.
- [17] Tran H. H., Nguyen-Trong N., Le T. T., et al, Wideband and multipolarization reconfigurable crossed bowtie dipole antenna, *IEEE Trans. Antenn. Propag.*, 65(2017), No. 12, 6968-6975.
- [18] Lu Y., Wang Y., Gao S., et al, Circularly polarised integrated filtering antenna with polarisation reconfigurability, *IET Microw., Antenn. & Propag.*, 11(2017), 2247-2252.
- [19] Fartookzadeh M., Mohseni Armaki S. H., Circular feeding network for circular polarisation reconfigurable antennas, *Electronics Lett.*, 55(2019), 677-679.
- [20] Cui Y. H., Zhang P. P., Li R. L., Broadband quad-polarisation reconfigurable antenna, *Electronics Lett.*, 54(2018), 1199-1200.